



The North African coastal low level wind jet: a high resolution view

Pedro M. M. Soares¹ · Daniela C. A. Lima¹ · Álvaro Semedo² · Rita M. Cardoso¹ · William Cabos³ · Dmitry Sein^{4,5}

Received: 23 January 2018 / Accepted: 9 September 2018
© Springer-Verlag GmbH Germany, part of Springer Nature 2018

Abstract

The North African coastal low-level jet (NACLLJ) lies over the cold Canary current and is synoptically linked to the Azores Anticyclone and to the continental thermal low over the Sahara Desert. Although being one of the most persistent and horizontally extended coastal wind jets, this is the first high resolution modelling effort to investigate the NACLLJ climate. The current study uses a ROM atmospheric hindcast simulation with ~25 km resolution, for the period 1980–2014. Additionally, the underlying surface wind features are also scrutinized using the CORDEX-Africa runs. These runs allow the building of a multi-model ensemble for the coastal surface flow. The ROM and the CORDEX-Africa simulations are extensively evaluated showing a good ability to represent the surface winds. The NACLLJ shows a strong seasonal cycle, but, unlike most coastal wind jets, e.g. the California one, it is significantly present all year round, with frequencies of occurrence above 20%. In spring and autumn, the maxima frequencies are around 50%, and reach values above 60% in summer. The location of maximum frequency of occurrence migrates meridionally from season to season, being in winter and spring upwind of Cap-Vert, and in summer and autumn offshore the Western Sahara. Analogously, the lowest jet wind speeds occur in winter, when the median is below 15 m/s. In summer, the jet wind speed median values are ~20 m/s and the maxima are above 30 m/s. The jet occurs at heights ~360 m. A momentum balance is pursued disclosing that the regional flow is almost geostrophic, dominated by the pressure gradient and Coriolis force. Over the jet areas the ageostrophy is responsible for the jet acceleration.

Keywords Regional climate modelling · Coastal low-level wind jet · Africa · CORDEX · ROM (REMO-OASIS-MPIOM) · Upwelling

Electronic supplementary material The online version of this article (<https://doi.org/10.1007/s00382-018-4441-7>) contains supplementary material, which is available to authorized users.

✉ Pedro M. M. Soares
pmsouares@fc.ul.pt

- ¹ Instituto Dom Luiz (IDL), Faculdade de Ciências, Universidade de Lisboa, Campo Grande, Ed. C8 (3.26), 1749-016 Lisbon, Portugal
- ² Department of Water Science and Engineering, IHE Delft, Delft, The Netherlands
- ³ Department of Physics, University of Alcalá, Alcalá de Henares, Madrid, Spain
- ⁴ Alfred Wegener Institute for Polar and Marine Research, Am Handelshafen 12, 27568 Bremerhaven, Germany
- ⁵ Shirshov Institute of Oceanology, Russian Academy of Science, 36 Nahimovskiy Prospect, Moscow 117997, Russia

1 Introduction

The pioneer study of Winant et al. (1988) identified the areas of the world where supercritical flow might be expected to occur within coastal marine regions; this is similar to asserting which offshore regions present favorable atmospheric conditions to the set-up of coastal low-level jets (CLLJ). The highlighted regions included the five eastern boundary current systems (EBCS) areas, i.e. California, Peru-Humboldt, Benguela, Canaries and West Australia, and two others, corresponding to the south Caribbean Sea and the Somalian Coast. Later, Ranjha et al. (2013) produced the first global CLLJs climatology, based on the ERA-Interim reanalysis (Dee et al. 2011), and confirmed the referred areas as regions where coastal wind jets occur. However, these authors indicated some differences with the global CLLJs pattern presented by Winant et al. (1988), namely the presence of an Iberian Peninsula coastal wind jet and a different location for the Somalian coastal jet. The last result was further confirmed in a follow-up study by Ranjha et al. (2015), where

the Somalian CLLJ (renamed Oman CLLJ by the authors) was acknowledged as a separate feature of the Findlater jet (Findlater 1969), both coinciding with the southwest Asian monsoon. In fact, they found that the Somalian CLLJ is not located offshore Somalia but along the coasts of Yemen and Oman, and co-exists with the Findlater jet. Moreover, Ranjha et al. (2013) does not identify the south Caribbean Sea jet as a CLLJ, since it has different generating mechanisms and properties, preventing it to be included in the group of the EBCS plus Oman CLLJs. Recently, Lima et al. (2018) presented a detailed analysis of the global coastal wind jet systems, based on four reanalyses: ERA-Interim, JRA-55 (Kobayashi et al. 2015), MERRA-2 (Bosilovich et al. (2015) and CFSR (Saha et al. 2010). These authors built the first multi-reanalysis ensemble for characterizing the present climate jets properties in a robust manner, illustrating the inherent CLLJ dissimilarities. In Lima et al. (2018) the CLLJs full seasonal cycle is explored, revealing that the annual cycle of the frequency of occurrence of coastal jets is stronger in the northern hemisphere than in the southern hemisphere. In the southern hemisphere, the Peru-Humboldt and Benguela coastal jets occurs during the entire year, with lower frequencies of occurrence in the austral winter. In the northern hemisphere, during the intermediate seasons the CLLJ regions display lower frequencies of occurrence, with the notable exception of the North African CLLJ.

The EBCS coastal jets occur in the eastern flanks of the mid-latitude oceans and are synoptically associated to the presence of a semi-permanent sub-tropical Anticyclone and an inland thermal low-pressure system. The Oman CLLJ is the exception, with a synoptic forcing associated with the Southeast Asia monsoon. Coastal wind jets occur within the maritime atmospheric boundary layer (MABL) and are locally enhanced by the land–ocean thermal contrast and the subsiding air above the MABL. Furthermore, coastal features, like coastal topography and capes, have a significant impact on the local/regional jet flow (Tjernström and Grisogono 2000; Chao 1985). Most of the CLLJ systems have been studied in depth, notably the California CLLJ the object of a higher number of studies (e.g. Burk and Thompson 1996; Parish 2000; Winant et al. 1988), and the North African and West Australia CLLJs the less investigated. Actually, both the North African and the Iberian wind jets emerge synoptically from the Azores Anticyclone but are linked to different continental thermal low-pressure systems, one over the Iberian Peninsula and the other over Northwest African Sahara Desert. Despite both jets being directly connected to the Azores Anticyclone system, the Iberian coastal jet has had much more attention, with several recent studies. Soares et al. (2014), and further Rijo et al. (2017), using a high resolution WRF regional climate simulations, extensively characterized the Iberian CCLJ features. They found that the Iberian coastal wind jet has a pronounced annual

cycle with large frequencies of occurrence in summer, up to 40%, and mean wind intensities around 15 m/s (at the jet maxima). In regard to the projected evolution of the Iberian CLLJ, in the context of climate change, Cardoso et al. (2016) and Soares et al. (2017a) showed, using regional climate simulations (at 50 km and 9 km, respectively), a consistent increase of its occurrence in summer and also in the intermediate seasons. Furthermore, in the case of the higher resolution simulation, the frequency of occurrence is projected to increase more than 15% by the end of the twenty-first century, in agreement with the RCP8.5 greenhouse gases scenario, when compared to present climate.

The North African CLLJ was never the focus of a detailed regional atmospheric modelling analysis, despite the fact that the aforementioned global studies, based on reanalyses, indicated that it is one of the coastal wind jets with higher yearly persistence (Ranjha et al. 2013; Lima et al. 2018), smaller annual cycle and larger spatial extension (Lima et al. 2018). Additionally, Semedo et al. (2016) suggested a significant increase of the persistency of this jet for winter in response to global warming. Even though the Iberian and the North African CLLJs are located in the same Eastern Atlantic basin, and share some forcing mechanisms and properties, they seem to have a lot that is diverse and still unclear.

It is important to stress that although some other studies mention the existence of the North African CLLJ, they identify it indirectly through surface wind analysis (Benazzouz et al. 2014a, b) and in relation to other regional atmosphere–ocean phenomena, like e.g. upwelling (Gómez-Gesteira et al. 2008). However, none of these investigations performed a detailed and systematic study of the North African CLLJ (NACLLJ). This paper aims at contributing to fill this gap.

In the current study, the first regional climate study focused on the North African coastal jet system is produced, based on a regional climate hindcast simulation, performed using the regional model ROM (Sein et al. 2015), at 25 km horizontal resolution. In this simulation the atmospheric component of ROM is run in stand-alone mode. The lateral boundary conditions and SST are taken from ERA-Interim. The 3-D and 3-hourly meteorological output of this climate run allows for a comprehensive investigation of the NACLLJ features aloft and near the surface. Additionally, we use the CORDEX-Africa (Coordinated Regional Climate Downscaling experiment; Giorgi et al. 2009) 0.44° resolution surface wind to characterize the surface flow and to offer a regional climate context to the ROM results. Firstly, an extensive evaluation of the ROM and of the CORDEX-Africa simulations is done, where the surface wind results are compared against the Cross-Calibrated Multi-Platform (CCMP; Atlas et al. 2011) dataset. Subsequently, the NACLLJ main properties for present climate are dissected, from the mean regional characteristics, to the annual and diurnal cycles and

as well the inter-annual variability. The NACLJ properties are analyzed in depth regarding the role of the main physical mechanisms, supported by the regional dynamical balance, i.e. the momentum budget of the coastal jet.

From here onwards the paper is organized as follows: in Sect. 2 the model, simulations and methods are introduced; Sect. 3 presents the results, including the model evaluation, the NACLJ main properties and the associated dynamical balance; and, in Sect. 4 a discussion and foremost conclusions are offered.

2 Model, data and methods

2.1 ROM model

The ROM model (Sein et al. 2015) emerged from the coupling, via OASIS coupler, of the following modelling components: the Regional atmosphere Model (REMO), the Max Planck Institute Ocean Model (MPIOM), the Hamburg Ocean Carbon Cycle model, and the Hydrological Discharge model. All these models are usually run in a global configuration, with the exception of REMO. The ROM acronym follows from REMO-OASIS-MPIOM. An atmospheric stand-alone hindcast simulation, covering the period 1980–2014, was performed with ROM using ERA-Interim as lateral boundaries and to prescribe SSTs. In this simulation REMO encloses a wide domain, including the full African continent and a large portion of the Atlantic Ocean (Fig. 1a). In this way, the NACLJ is located away from the region that is influenced by the boundary conditions.

2.2 CORDEX-Africa simulations

The CORDEX-Africa simulations (Hewitson et al. 2012; Nikulin et al. 2012) were developed under the Coordinated Regional Climate Downscaling (CORDEX) effort, which promoted a considerable number of regional climate model (RCM) simulations at continental scales (Giorgi et al. 2009). Within the CORDEX-Africa a common domain covering the African continent was selected (Fig. 1b). Six RCMs, described in Table 1, were used to simulate the present African climate, between 1990 and 2008, with a horizontal resolution of 0.44° . All simulations were forced with ERA-Interim as boundary conditions (hence they are hindcast simulations) and are stand-alone atmosphere runs. Within the MABL only the daily surface wind speed at 10 m height is accessible and is here used to characterize, in a more robust way, the surface atmospheric flow over the NACLJ region. It is important to emphasize that surface wind data at daily sampling is not suitable to characterize the CLLJ, but only the associated mean surface flow in the jet area. Furthermore, due to the scarcity of observational data in the region the inclusion of this RCMs surface wind data provides further insight on the relative quality of the ROM performance. The CORDEX-Africa data is available in the Portal ESGF (Earth System Grid Federation; <http://esg-dn1.nsc.liu.se/esgf-web-fe/live>, last accessed on 21/07/2017). In order to differentiate the simulations, an institution acronym was assigned to each model dataset (Table 1).

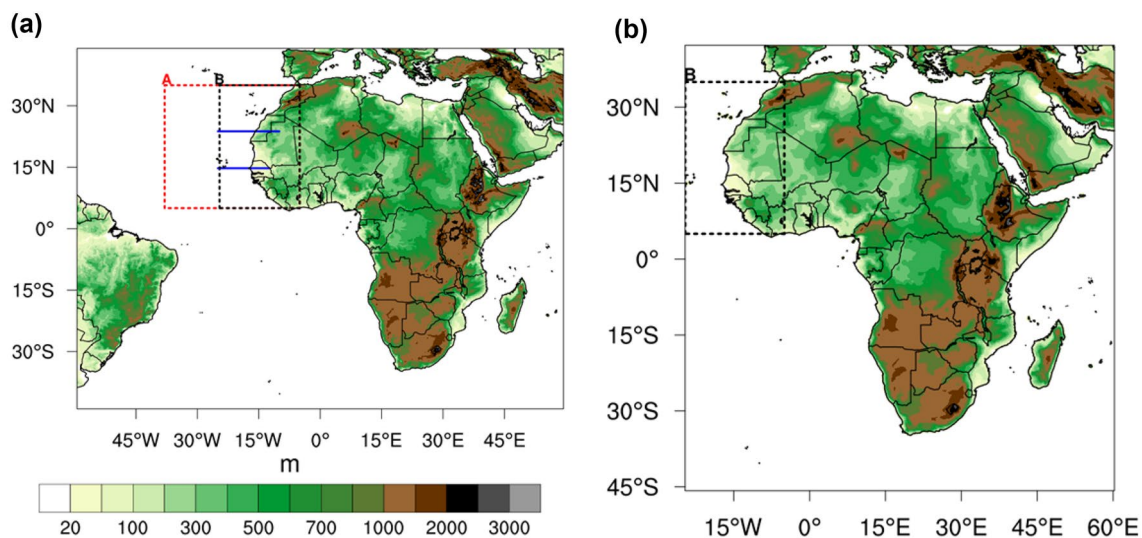


Fig. 1 **a** ROM simulation domain (full map area), **b** CORDEX-Africa common domain (full map area). The dashed red and black lines delimit the areas of analysis regarding the North African coastal low

level jet and model evaluations, respectively. The blue line marks two representative cross-sections

Table 1 CORDEX-Africa regional climate models forced by ERA-Interim Reanalysis considered in the present study, along with the responsible institution, the acronym for each model (RCM)

AFR-CORDEX regional climate model	Acronym	Institution	References
CCLM4-8-17	CLM	Climate Limited-area Modelling Community	Rockel et al. (2008)
HIRHAM5	DMI	Danish Meteorological Institute	Christensen et al. (2007)
RACMO22E	KNMI	Koninklijk Nederlands Meteorologisch Instituut	Van Meijgaard et al. (2008)
REMO2009	MPI	Helmholtz-Zentrum Geesthacht, Climate Service Center, Max Planck Institute for Meteorology	Jacob et al. (2001)
RCA4	SMHI	Swedish Meteorological and Hydrological Institute	Samuelsson et al. (2011)
CRCM5	UQAM	University of Quebec in Montreal	Martynov et al. (2013)

All models at 0.44° resolution

2.3 Observations

The Cross-Calibrated Multi-Platform (CCMP) surface wind fields were used to evaluate the RCM hindcast simulations performance. The CCMP data set (Atlas et al. 2011) was developed by NASA (National Aeronautics and Space Administration). This wind product combines cross-calibrated satellite winds, from microwave satellite instruments, and variational analysis method. In situ measurements and ECMWF reanalysis were used in the variational analysis method. The CCMP has 0.258° of horizontal resolution and 6-h temporal resolution. The output spans the period from July 1987 to June 2011 without gaps.

2.4 Model evaluation

In order to perform an analysis of the North African CLLJ, an evaluation of the RCMs results is crucial (Soares et al. 2012, 2017c; Nogueira et al. 2018). Since the ROM and the CORDEX-Africa simulations and the observational data sets have different resolutions, the higher resolution daily wind speed from the ROM model was interpolated using nearest grid point, to the 0.25° observational grid (CCMP). In order to evaluate the CORDEX-Africa wind speeds, the model results and the CCMP data were both interpolated to a common regular grid at 0.44° resolution, using nearest point. The common time period between RCM simulations and observations defines the time period for near surface wind speed evaluation 1990–2008.

For all the available points and time scales (daily, monthly, seasonal and yearly) the following standard statistics for wind speed are computed (the number of the related equation, presented below, are indicated in brackets): bias (1), percent bias [bias%; (2)], mean absolute error [MAE; (3)], mean absolute percentage error [MAPE; (4)], normalized standard deviation (σ_n ; (5)), Willmott-D Score (D ; (6)), and spatial correlation (r ; (7)).

$$Bias = \frac{1}{N} \sum_{k=1}^N (p_k - o_k) \tag{1}$$

$$Bias\% = \frac{\sum_{k=1}^N (p_k - o_k)}{\sum_{k=1}^N o_k} \times 100 \tag{2}$$

$$MAE = \frac{1}{N} \sum_{k=1}^N |p_k - o_k| \tag{3}$$

$$MAPE = \frac{\sum_{k=1}^N |p_k - o_k|}{\sum_{k=1}^N o_k} \times 100 \tag{4}$$

$$\sigma_n = \frac{\sigma_p}{\sigma_o} = \frac{\sqrt{\frac{1}{N} \sum_{k=1}^N (p_k - \bar{p})^2}}{\sqrt{\frac{1}{N} \sum_{k=1}^N (o_k - \bar{o})^2}} \tag{5}$$

$$D = \begin{cases} 1 - \frac{\sum_{k=1}^N |p_k - o_k|}{2 \sum_{k=1}^N |o_k - \bar{o}|}, & \text{if } \sum_{k=1}^N |p_k - o_k| \leq 2 \sum_{k=1}^N |o_k - \bar{o}| \\ \frac{2 \sum_{k=1}^N |o_k - \bar{o}|}{\sum_{k=1}^N |p_k - o_k|} - 1, & \text{if } 2 \sum_{k=1}^N |o_k - \bar{o}| < \sum_{k=1}^N |p_k - o_k| \end{cases} \tag{6}$$

$$r = \frac{\sum_{k=1}^N (o_k - \bar{o}) - (p_k - \bar{p})}{\sqrt{\sum_{k=1}^N (o_k - \bar{o})^2 \sum_{k=1}^N (p_k - \bar{p})^2}} \tag{7}$$

The number of observed/modelled events is represented by N , o_k and p_k are the observed/modelled values, and \bar{o} and \bar{p} are the mean of the observed/modelled values. The Willmott D score (Willmott et al. 2012) assesses not only differences in the mean, but also in the standard deviation. A perfect skill is obtained when $D = 1$ whilst $D = -1$ is

achieved when there is no skill. Additionally, the daily wind speed probability distribution functions (PDFs) are analysed resorting to the PDF matching scores (S , Perkins et al. 2007; Boberg et al. 2009) and the Yule–Kendall skewness measure (YK; Ferro et al. 2005), such as:

$$S = \int \min(E_M, E_O) \tag{8}$$

$$YK = \left[\frac{(P_{95} - P_{50}) - (P_{50} - P_5)}{(P_{95} - P_5)} \right]_{model} - \left[\frac{(P_{95} - P_{50}) - (P_{50} - P_5)}{(P_{95} - P_5)} \right]_{obs} \tag{9}$$

where P represents the percentiles, E_M and E_O are the empirical distribution function of the model and observed pooled sample, respectively. The first score provides an integral measure of the overlap between the observed and modelled values. A perfect overlap is obtained when $S = 1$ or 100%. The Yule–Kendall skewness measure indicates the difference between the modelled and observed PDF skewness, thus its values should be close to zero for a good match between the PDFs shape.

Finally, in agreement with the common assumption that multi-model ensembles may represent in an improved way the regional climate (Soares et al. 2015, 2017b; Cardoso et al. 2018) a multi-model ensemble was constructed from all CORDEX-Africa models, defining as EnsFull, in which the weights are equal for all models ($1/[num. of models]$), i.e. for the ensemble, the mean measures are averaged. The PDFs are obtained by

$$PDF(x) = \sum_{i=1}^N PDF(x)_i w_{g_i} \quad (N = no\ of\ models) \tag{10}$$

where w_{g_i} is the model weight.

2.5 CLLJ analysis and dynamical balance

The detailed analysis of the NACLLJ is performed only with the ROM simulation, since the CORDEX-Africa RCMs model levels results are not available. The considered period corresponds to the full ROM simulation time span, 1980–2014. Following Ranjha et al. (2013) and Lima et al. (2018), the vertical wind speed and temperature profiles are examined using a CLLJ detection algorithm. This method identifies a CLLJ occurrence, when the following criteria are met:

- The height of the jet maximum is within the lowest 1 km in the vertical;

- The wind speed at the jet maximum is at least ~20% higher than the wind speed at the surface;
- The wind speed above the jet maximum decreases to below ~80% of the wind speed at the surface (i.e. a ~20% falloff) before reaching 5 km above its maximum;
- The jet maximum is within or at the top of the MABL temperature inversion;
- The maximum temperature does not occur at the base (rejection of surface-based inversion).

The analysis of the NACLLJ annual and diurnal cycles, its inter-annual variability and, frequency of occurrence, as well as its jet wind speed are presented. The vertical and horizontal features of the coastal jet are also investigated.

The momentum budget equations are scrutinized to better understand the main physical mechanisms that determine the NACLLJ seasonal properties. The zonal and meridional momentum equations are:

$$\frac{\partial \bar{u}}{\partial t} = - \left(\bar{u} \frac{\partial \bar{u}}{\partial x} + \bar{v} \frac{\partial \bar{u}}{\partial y} + \bar{w} \frac{\partial \bar{u}}{\partial z} \right) + f \bar{v} - \frac{1}{\rho_0} \frac{\partial \bar{P}}{\partial x} + v \left(\frac{\partial^2 \bar{u}}{\partial x^2} + \frac{\partial^2 \bar{u}}{\partial y^2} + \frac{\partial^2 \bar{u}}{\partial z^2} \right) - \left(\frac{\partial(\overline{u'u'})}{\partial x} + \frac{\partial(\overline{u'v'})}{\partial y} + \frac{\partial(\overline{u'w'})}{\partial z} \right) \tag{11}$$

$$\frac{\partial \bar{v}}{\partial t} = - \left(\bar{u} \frac{\partial \bar{v}}{\partial x} + \bar{v} \frac{\partial \bar{v}}{\partial y} + \bar{w} \frac{\partial \bar{v}}{\partial z} \right) - f \bar{u} - \frac{1}{\rho_0} \frac{\partial \bar{P}}{\partial y} + v \left(\frac{\partial^2 \bar{v}}{\partial x^2} + \frac{\partial^2 \bar{v}}{\partial y^2} + \frac{\partial^2 \bar{v}}{\partial z^2} \right) - \left(\frac{\partial(\overline{v'u'})}{\partial x} + \frac{\partial(\overline{v'v'})}{\partial y} + \frac{\partial(\overline{v'w'})}{\partial z} \right) \tag{12}$$

where \bar{u} , \bar{v} and \bar{w} are the mean wind speed components (zonal, meridional, and vertical, respectively), and u' , v' and w' are the turbulent wind speed components. The seasonal horizontal momentum budget was computed at the height correspondent to the jet height frequency of occurrence mode. In both equations, from left to right, the terms correspond to local time change, advection (zonal, meridional and vertical), Coriolis, pressure gradient, diffusion and turbulence (to simplify these last two terms are aggregated as mixing).

3 Results

3.1 Models surface wind evaluation

The evaluation of the surface wind speeds from the ROM hindcast, the individual CORDEX-Africa RCM hindcasts and full CORDEX-Africa multi-model ensemble, is shown in Fig. 2, where the biases (%) and MAPEs at different time scales (monthly, seasonally and yearly) are shown. In Table 2

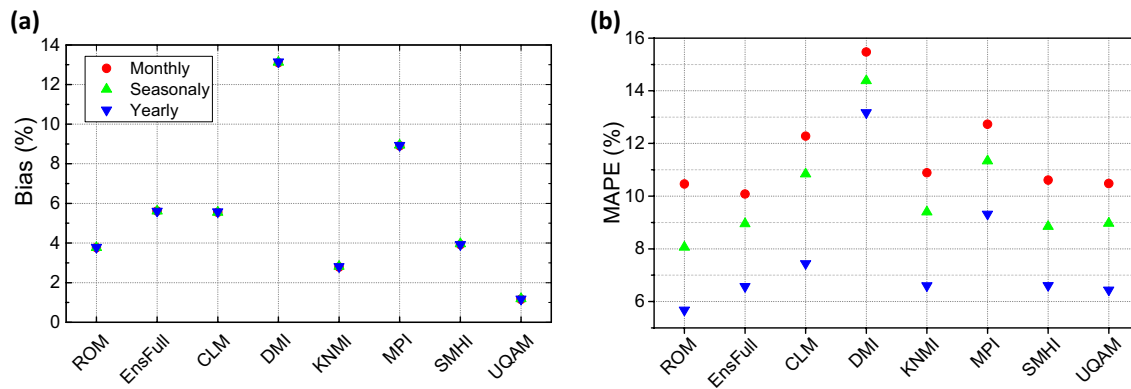


Fig. 2 Error measures of the ROM and CORDEX-Africa simulations surface wind speeds (10 m) against the CCMP dataset for the area delimited in dashed black in Fig. 1. EnsFull corresponds to the CORDEX-Africa multi-model ensemble. The error measures are

the normalized bias (bias%) and the mean absolute percentage error (MAPE). The errors are computed for different time periods of near surface wind speed (monthly in red, seasonally in green and yearly in blue)

Table 2 Statistical errors and skill scores comparing the surface winds of the ROM and CORDEX-Africa RCM simulations against the CCMP wind dataset

RCMs	Bias (%)	MAPE%	Normalized Standard Deviation	Wilmott-D	Correlation	S	Yule-Kendall
ROM	3.77	24.41	1.02	0.66	0.69	94.23	-0.006
	3.77	8.06	0.93	0.74	0.86		
0.44°							
CLM	5.55	20.76	1.11	0.68	0.77	91.82	0.036
	5.55	10.84	1.11	0.70	0.87		
DMI	13.1	23.72	1.06	0.63	0.70	87.67	-0.012
	13.1	14.38	1.00	0.61	0.87		
KNMI	2.79	18.74	1.06	0.71	0.78	94.74	-0.010
	2.79	9.40	1.19	0.74	0.90		
MPI	8.91	21.27	1.02	0.67	0.74	91.69	-0.006
	8.91	11.34	0.91	0.69	0.87		
SMHI4	3.92	19.92	1.05	0.69	0.78	95.69	0.004
	3.92	8.85	1.09	0.75	0.90		
UQAM	1.16	19.07	0.99	0.70	0.77	94.32	0.023
	1.16	8.98	1.04	0.75	0.88		
EnsFull	5.61	16.29	0.96	0.75	0.86	94.66	0.035
	5.61	8.00	1.06	0.76	0.91		

These errors allow the ranking of the CORDEX-Africa RCMs and the ROM simulation. From the CORDEX-Africa runs a multi-model ensemble is built and its errors are also displayed in the last row. The errors are: daily (left) and seasonal (right) bias, MAPE, normalized standard deviation and Wilmott-D score, spatial correlation and daily S pdf matching skill score and Yule-Kendall score

the daily and seasonal errors are listed for all error metrics aforementioned. All these errors are computed against the CCMP dataset. The ROM and CORDEX-Africa simulations percent biases range from 1 to 13%, yet most of the models show errors less than 10%. UQAM, KNMI and ROM models display the smallest %bias: 1, 3 and 4%, respectively. More importantly, the MAPE, which is not affected by error compensation, indicates that ROM is the best performing model

for the three temporal scales. Additionally, it is relevant to stress that ROM is compared at a higher resolution than CORDEX-Africa simulations. Although it is fair to say that the CORDEX-Africa RCMs display roughly similar errors, and consequently it is not a surprise to realize the good performance of the full multi-model ensemble, particularly at the monthly MAPE. DMI reveals the worst MAPE, from the monthly to the yearly timescale.

A broader view of the RCMs performance, including other error measures, for the daily and seasonal scales, reveals an overall good representation of the offshore surface wind speed in the area of interest, even at ~ 50 km resolution. All models present an overestimation of surface winds, with positive biases. The CORDEX-Africa models, in particular KNMI, SMHI4 and UQAM, display good skills, from bias to the S score. For example, at the daily and seasonal scales, KNMI shows a bias of 2.79%, corresponding to a MAPE of $\sim 19\%$ and $\sim 9\%$, respectively, and slightly overpredicts the variability (1.06 and 1.19 normalized standard deviation for each timescale). This is summarized in the high Willmott D score, 0.71 (daily) and 0.74 (seasonally). The good spatial agreement between CCMP and KNMI is given by the daily and seasonal spatial correlations with values of 0.78 and 0.90, respectively. KNMI's wind speed PDF is also consistent in shape and intensity, with low Yule–Kendall (-0.01) and high S score, 95%. As expected, the full multi-model ensemble outperforms the individual RCMs in almost all error measures. For example, it is striking that the multi-model ensemble daily MAPE and spatial correlation are $\sim 16\%$ and 0.86, respectively. More importantly, the ROM hindcast simulation reveals similar errors to the CORDEX-Africa RCMs. In some cases, the ROM model ranks as one of the best performing models, like for the seasonal MAPE, normalized standard deviation and S, and in other measures reveals somewhat a poor performance, as for example in the case of daily MAPE and correlation. This is probably linked to the fact of comparing directly the ROM wind results against the CCMP at higher resolution (0.25°) and not, as for the CORDEX-Africa results, at the aggregated resolution (0.44°).

The seasonal surface mean wind speeds (at 10 m height) results from the ROM and the CORDEX-Africa multi-model ensemble simulations, for present climate, are displayed in Fig. 3. Overall, the seasonal wind speed patterns are comparable, with some local small differences. The seasonal surface wind speeds offshore North Africa appear unequivocally connected to the coastal processes that set the North African coastal jet, namely the high pressure system of Azores and a thermal low over land. These force an alongshore equatorward surface wind all year-round, more persistent and intense in summer. In winter, the surface wind speeds are, on average, around 6 m/s, north of Guinea and ~ 3 m/s in the southern offshore regions. The surface wind speed is enhanced, especially in connection with the main coastal irregularities, like Cap Blanc in the intermediate seasons and Cape Bojador and Ghir in summer. Attaining seasonal mean values in summer above 10 m/s, in the offshore areas of Cap Ghir. The differences between the datasets are presented in supplemental material (Fig. S1). As revealed by Table 2 and Figs. 2 and 3, ROM and the full multi-model ensemble overpredict the surface flow, especially in coastal

areas, where the flow is constrained by coastal irregularities and where the wind is stronger, linked to the presence of the coastal low-level jet. Li et al. (2013) comparing CCMP winds with ship wind speed measurements refers that CCMP show large positive biases under weak wind regimes, good agreement under moderate wind regimes, and large negative biases under high wind regimes. The jet regions are areas with high wind regimes and this may partially explain the large models overestimation when compared with CCMP. Furthermore, CCMP has known problems in coastal regions, due to backscatter from land, which contaminates the wind speed measurements and results in wind speed underrepresentation (Tang et al. 2004; Soares et al. 2014). Finally, it is worth to mention that the comparison of the surface wind direction given by the ROM run and the CCMP dataset (not shown) also reveals a good agreement.

3.2 NACLLJ properties

The large-scale atmospheric flow over the Atlantic Ocean/North Africa region is directly linked to the semi-permanent Azorean High pressure system and the inland thermal low. These large-scale features are especially intense in summer, and in winter the inland thermal low is absent (Fig. S2). Hence, the offshore atmospheric flow is predominantly equatorward and along-shore. The ocean-land thermal contrast originates a thermally direct circulation which prompts the occurrence of the coastal low-level jet through thermal wind adjustment. For the subsequent analysis only ROM data is used as for CORDEX-Africa RCMs simply surface winds are available.

Figures 4a and 5 depict the NACLLJ frequency of occurrence annual cycle (Fig. 4a at monthly scale for the area of interest, and Fig. 5 regional maps at the seasonal scale). The NACLLJ shows a strong annual cycle, but unlike most CLLJs, e.g. California and Iberia (Ranjha et al. 2013; Soares et al. 2014; Semedo et al. 2016; Lima et al. 2018) it is significantly present all year round, with frequencies of occurrence above 20% in some winter offshore areas. At the monthly scale the absolute maximum values reach 99% (i.e. there is a CCLJ in a particular point almost every day in a month of June) and the regional median values attain 23% in August. The minimum values take place in December with absolute minimum and regional mean values of 0% and 5%, respectively.

As previously stated, the Iberian CLLJ and the NACLLJ are intrinsically linked, since both depend on the Azores High synoptic forcing. However, these CLLJs are considered two different CLLJ systems as they depend on two different inland low pressure systems and their continuity is disrupted by the Gibraltar easterly flow (Ranjha et al. 2013; Semedo et al. 2016; Lima et al. 2018). Following this assumption, it can be seen that the spatial coverage of the CCLLJ is still

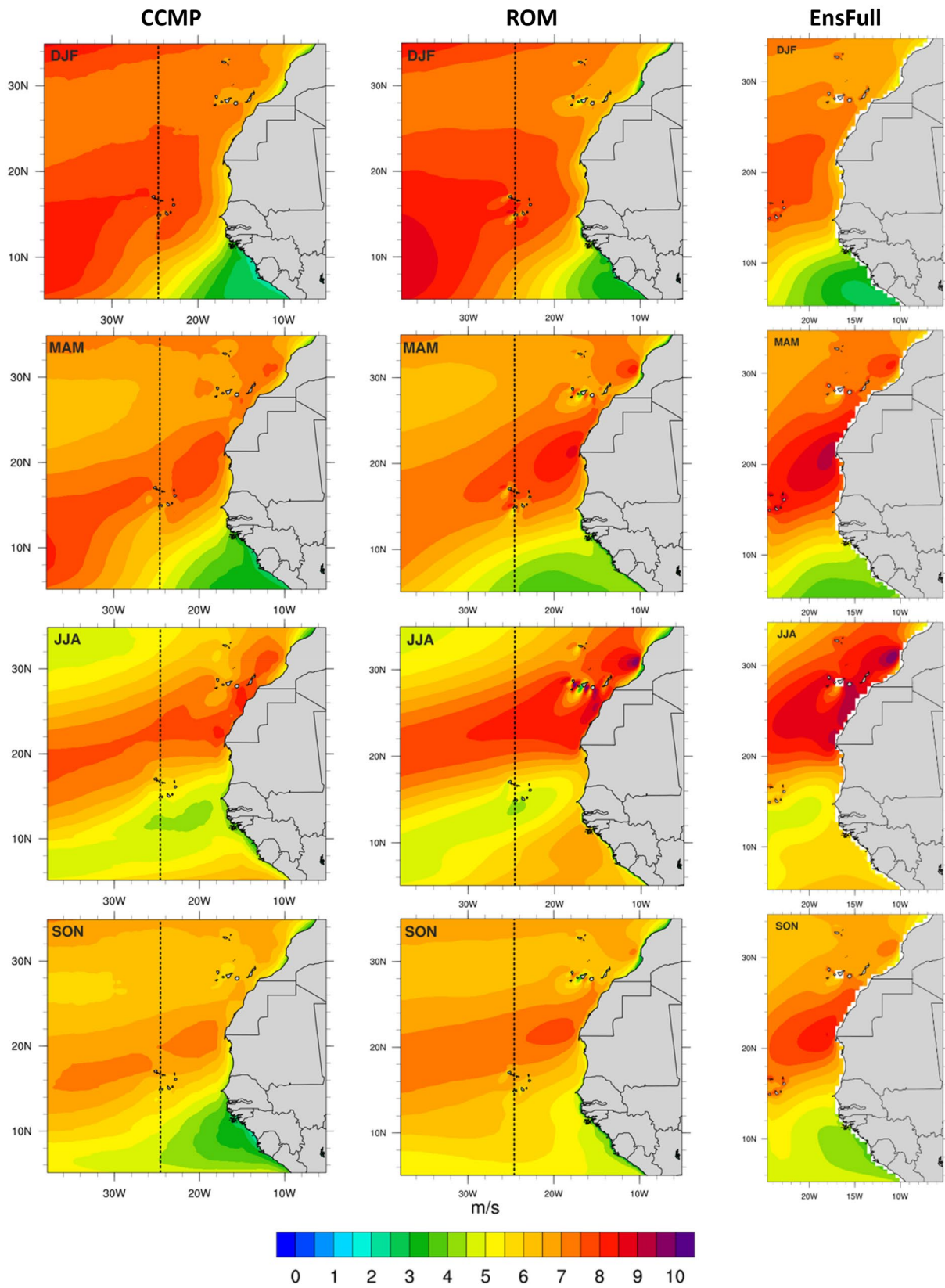


Fig. 3 Seasonal surface mean wind speeds for present climate (1990–2008), from the CCMP observational dataset, the ROM simulation and the CORDEX-Africa full multi-model ensemble

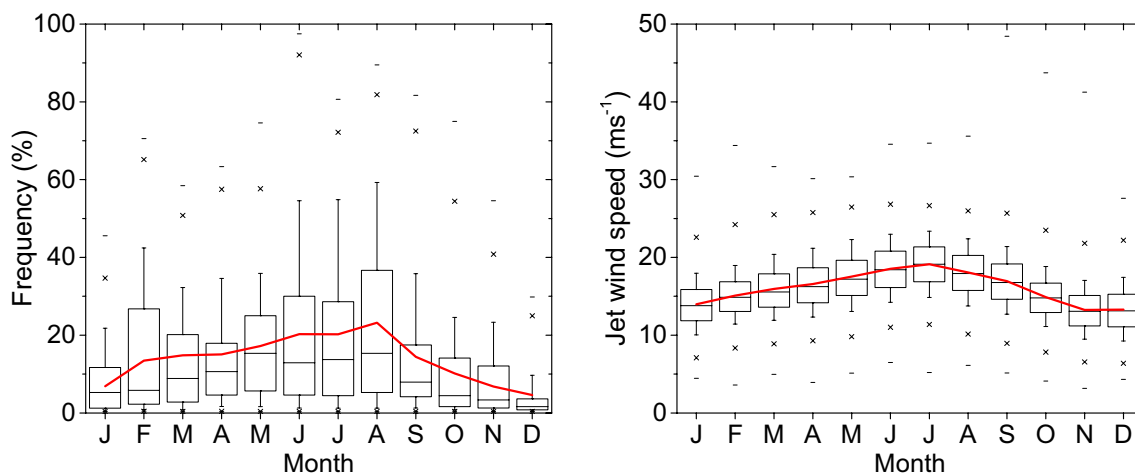


Fig. 4 Annual Cycle of the Canaries low-level jet: (left) the mean jet frequency of occurrence and (right) the mean jet wind speed, results from the ROM simulation at 25 km resolution. Individual boxes span from the 25th to the 75th percentile, with the median represented by

a straight line and the mean represented by a red line. The whisker spans from 10th to 90th. The 99th and 1st percentiles are denoted by crosses, with the maximum and minimum indicated by a dash

remarkable, extending from the north offshore regions of Morocco (in all seasons with the exception of winter), to the southern offshore areas of the Guineas (Fig. 5). The offshore extension of the CLLJ is also striking, influencing areas more than 1000 km off the coast.

In winter, a large area, which extends from the southern Western Sahara coastal regions to Guinea-Bissau, is under the influence of the coastal jet about 15% of the time, and in spring its persistency and horizontal extension greatly increases. During this season, the maximum frequency of occurrence is $\sim 50\%$, located upwind of Cap-Vert, but almost all coastal areas are affected by the jet to some extent. During summer, the highest frequency of occurrence areas migrate northerly, increasing to more than 60% offshore areas Western Sahara, and 50% downwind of Cape Ghir. In spring and summer, the NACLLJ offshore extension is rather remarkable, reaching more than 1200 km, with a clear impact on the Cape Verde Islands. Finally, there is a decrease in the frequency of the coastal jet in autumn, reaching values below 45% in the southern coastal region of the Western Sahara.

The jet wind speeds show a sharp seasonal cycle (Fig. 4; at monthly scale), where winter jet wind speeds are mostly below 15 m/s, and increase steadily throughout spring to summer. In July, the 25th percentile of the jet wind is above 15 m/s, and the percentile 90th is around 25 m/s. In autumn, the jet wind speeds decrease until November, when jet wind speeds are similar to winter months.

The seasonal jet wind speed and jet height histograms are shown in Fig. 6. The lowest jet wind speeds occur in winter, when the median jet wind speed is below 15 m/s and the maximum jet wind speeds do not reach 28 m/s.

In the intermediate seasons a shift for higher jet wind speeds occurs, where both medians are above 15 m/s and a larger persistency of values above 20% can be found. The increased jet wind speeds appear even greater in summer, when median values amount to around 20 m/s. Both in autumn and summer, the jet wind speed maxima are above 30 m/s, but not in spring. For all seasons, the most prevalent jet wind speeds occur with similar frequencies, of around 25%.

The heights of jet occurrence are quite similar from season to season (Fig. 6). In fact, the jet is always more prevalent on heights around 360 m, with frequencies of occurrence around 65% in winter and spring, and 70% in summer and autumn. In all seasons the second preferable heights of jet occurrence are around 200 m ($\sim 20\%$).

The seasonal wind roses show that the jet winds are predominantly parallel to the coast (Fig. 7). In summer, 80% of the jets have a Northeasterly direction (30% from NNE and 50% NE), with a prevalent wind speed between 12 and 16 m/s. The surface wind speed is obviously lower, between 8 and 12 m/s and chiefly from NNE. In the intermediate seasons the NE is still predominant, but the NNE and ENE together have an equivalent frequency of occurrence. As in summer, the surface wind speed is rotated to more northerly direction. In winter the easterly component from the trade winds has a stronger influence and the NE and ENE have similar frequencies ($\sim 30\%$). The dominant wind speed is still 12–16 m/s. Near the surface the wind is most frequently from NE.

As expected, the diurnal cycle of the NACLLJ reveals a strong seasonality (Fig. 8). Firstly, both winter and summer show a marked diurnal cycle of both the jet frequency

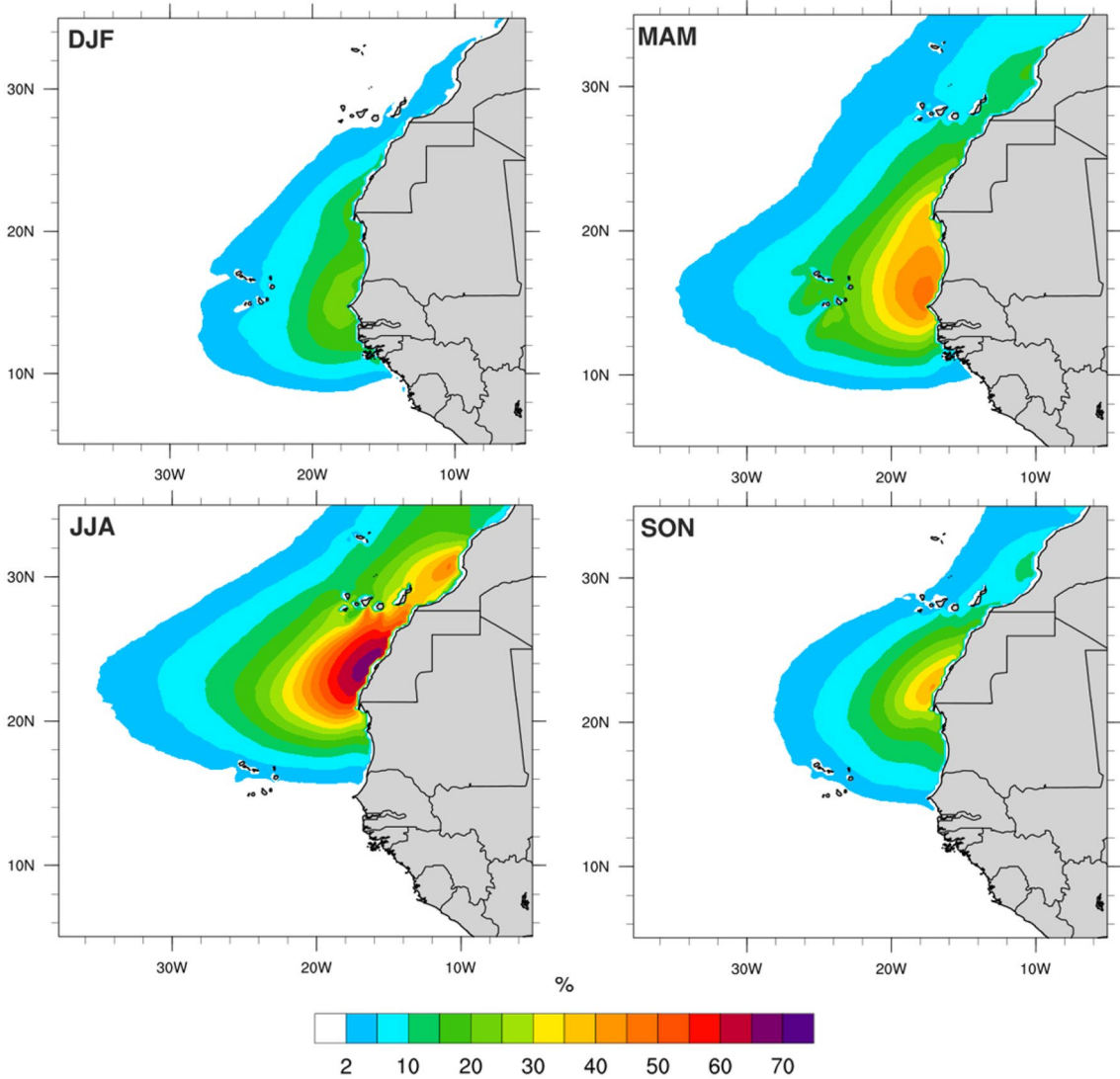


Fig. 5 Maps of seasonal coastal jet frequency of occurrence (%), DJF-winter, MAM-spring, JJA-summer and SON-autumn, results from the ROM hindcast simulation

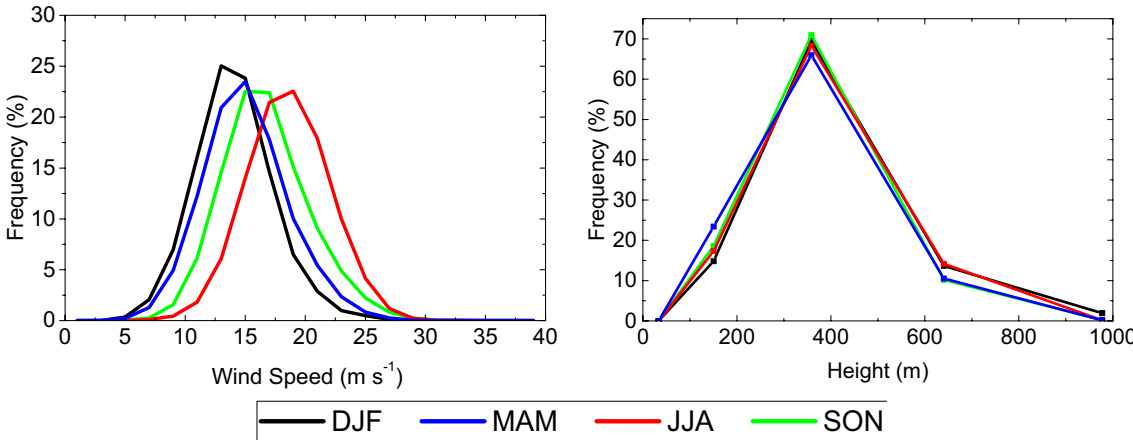
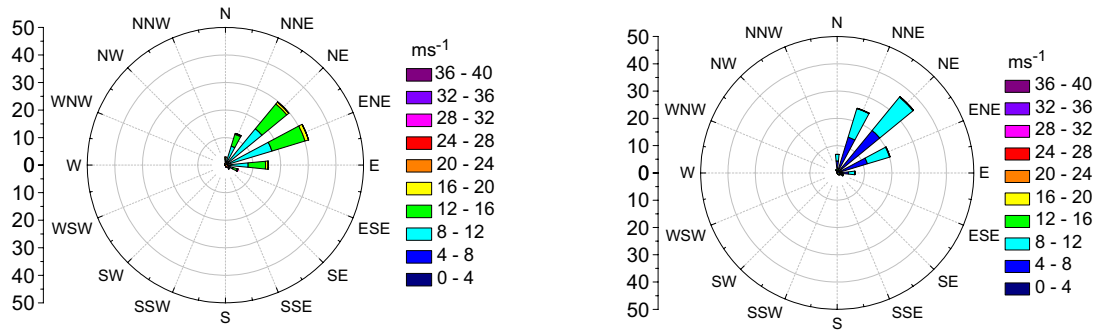
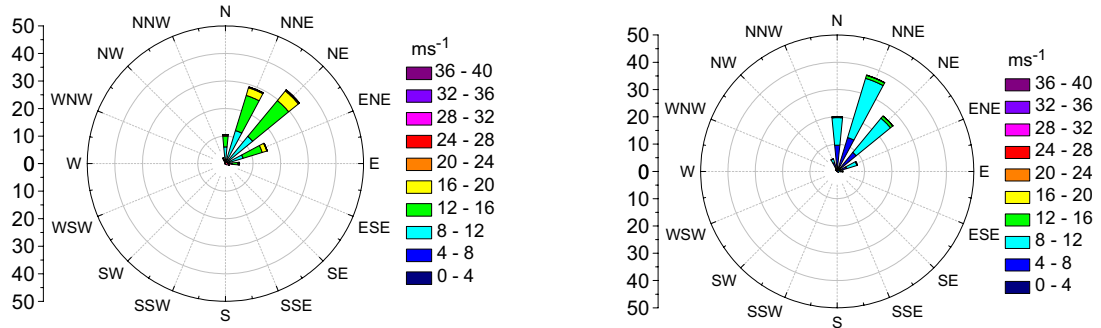


Fig. 6 Seasonal coastal low level jet wind speed histograms (left) and jet height histograms (right)

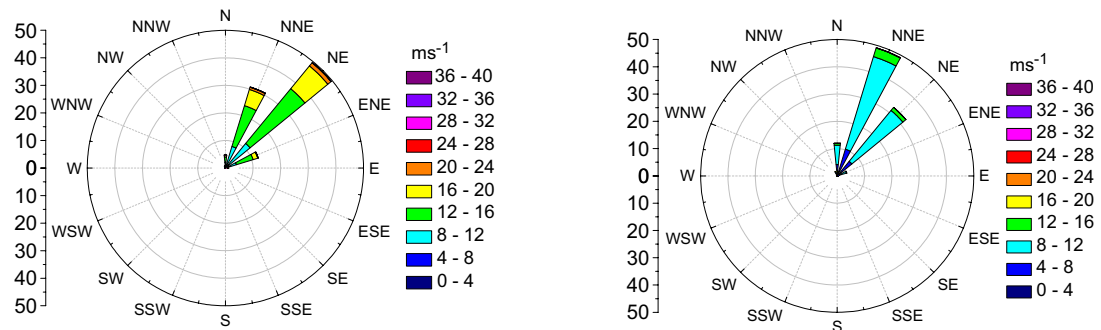
DJF



MAM



JJA



SON

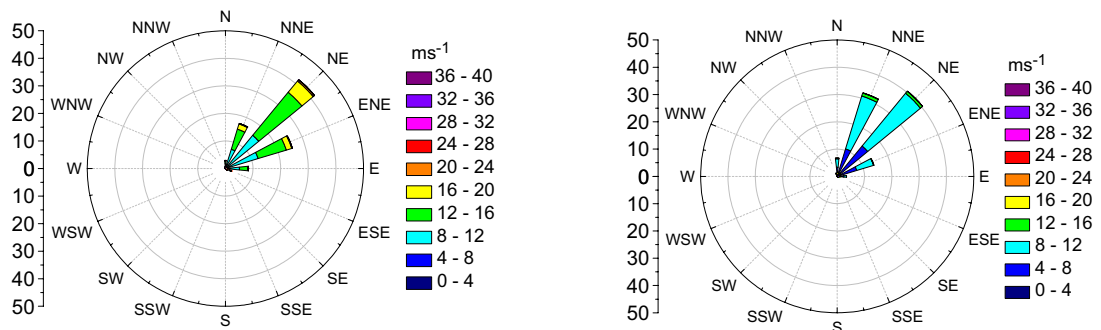


Fig. 7 Seasonal wind roses at jet height (left) and surface winds when jet occurs (right)

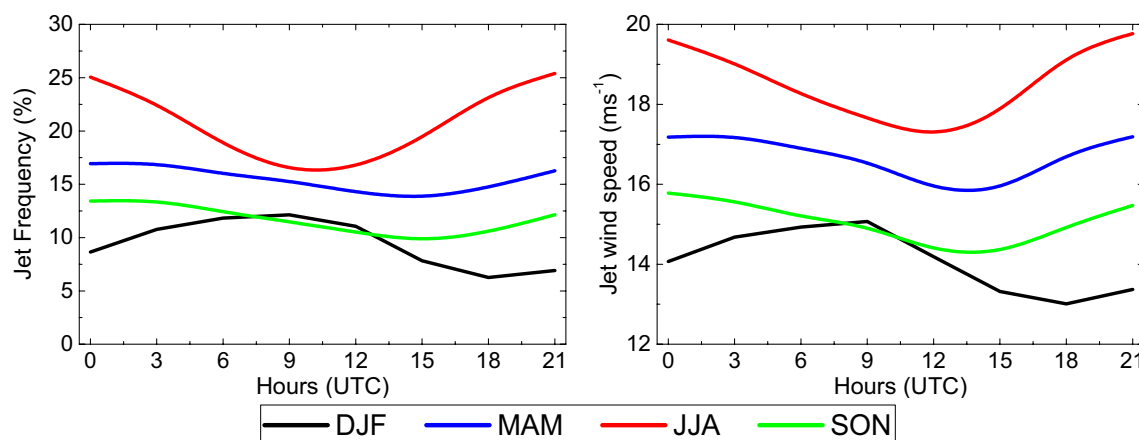


Fig. 8 Diurnal Cycle of the jet frequency of occurrence (left) and of the jet wind speed (right)

of occurrence and its wind speed. Contrariwise, spring and autumn have an associated smaller diurnal cycle of the jet frequency and of jet wind speed. In summer, the diurnal amplitude of the frequency of occurrence is around 10%, being minimum between 9 and 12 UTC (~15%) and maximum between 21 and 0 UTC (~25%). A similar diurnal cycle can be found for the jet wind speed, but evolving from around 17 m/s at 12 UTC to 20 m/s at 21 UTC. This sharp diurnal cycle is linked to the diurnal cycle of the inland radiative heating that enhances the Sahara thermal Low and the thermal contrast between the ocean and land, forcing the maximum of the jet flow to occur late evening and early night. In the intermediate seasons a slight shift of the maximum and minimum of jet occurrence can be seen at 00 UTC and 15–18 UTC, respectively. However, the frequency amplitude can be seen as small (~3%). In these seasons the jet wind speed minima are at ~15 UTC and the maxima at ~00 UTC, and the jet wind speed diurnal amplitude is also small (around 1 m/s). In winter the jet maximum frequency of occurrence happens at 9 UTC (~12%) with the maximum jet wind speeds (15 m/s).

3.3 NACLLJ dynamical balance

Figure 9 depicts two cross-sections with the mean seasonal isotachs, isobars and isentropes, when the jet occurs (see Fig. 1 for cross section lines). Common to all seasons is the upward slope of the isentropes, from east to west, above the well-mixed MABL. The elongated jet wind speed structure clearly follows this thermal field, revealing the main physical mechanism of wind jet acceleration associated to the baroclinic structure within the MABL. The thermal contrast between land and ocean induces a thermally direct circulation which enhances the isothermal slope near the coast and generates a frontal structure in the MABL. The horizontal temperature gradient and the associated thermal wind

adjustment gives rise to the maxima of jet wind speed in the inversion layer (Fig. 8 in Parish 2000). Above the MABL inversion the horizontal temperature gradient decreases rapidly hence the fast wind speed decrease.

The NACLLJ seasonal cycle and its migration through Northwest Africa is also visible and interesting to follow in Fig. 9. The northern cross-section (at 23.76°N; Fig. 1a) displays the archetypal coastal jet seasonal cycle, from its smaller intensity/frequency and offshore extension in winter to its maximum values and offshore influence in summer. The mean coastal jet speeds (wind speed at the jet maxima) increase from ~10 m/s in winter to around 15 m/s in summer. As aforementioned, these jet maxima are straightly linked to the strikingly compressed adiabatic lines near the coast, in response to the well-mixed MABL, the aloft subsidence due to the Azores Anticyclone, the thermal low over land and the induced direct thermal circulation. Contrastingly, the southern cross-section depicts a different seasonal cycle, where the maximum mean CLLJ wind speeds occur in spring. This is closely linked to the enhanced horizontal temperature gradient (Fig. 9b) and to the inland thermal low at these latitudes (Fig. S2).

As previously seen, the most prevalent height of jet occurrence is around 360 m (Fig. 6). Therefore, the seasonal momentum balance terms (meridional and zonal) when jet occurs, in agreement with Eqs. 11 and 12, are computed at this level (Figs. 10, 11, respectively). Additionally, the corresponding wind speeds and ageostrophic components are shown in Fig. 12.

The northwest African coast is rather irregular, in conjunction a large portion of it has a roughly 45° angle with latitudes and therefore a predominant alongshore north-easterly flow (Fig. 7). Hence, the two momentum balance components are expected to present more similarities, when compared, for example, with the Chilean coast which is crudely north–south. In the latter, Muñoz and Garreaud

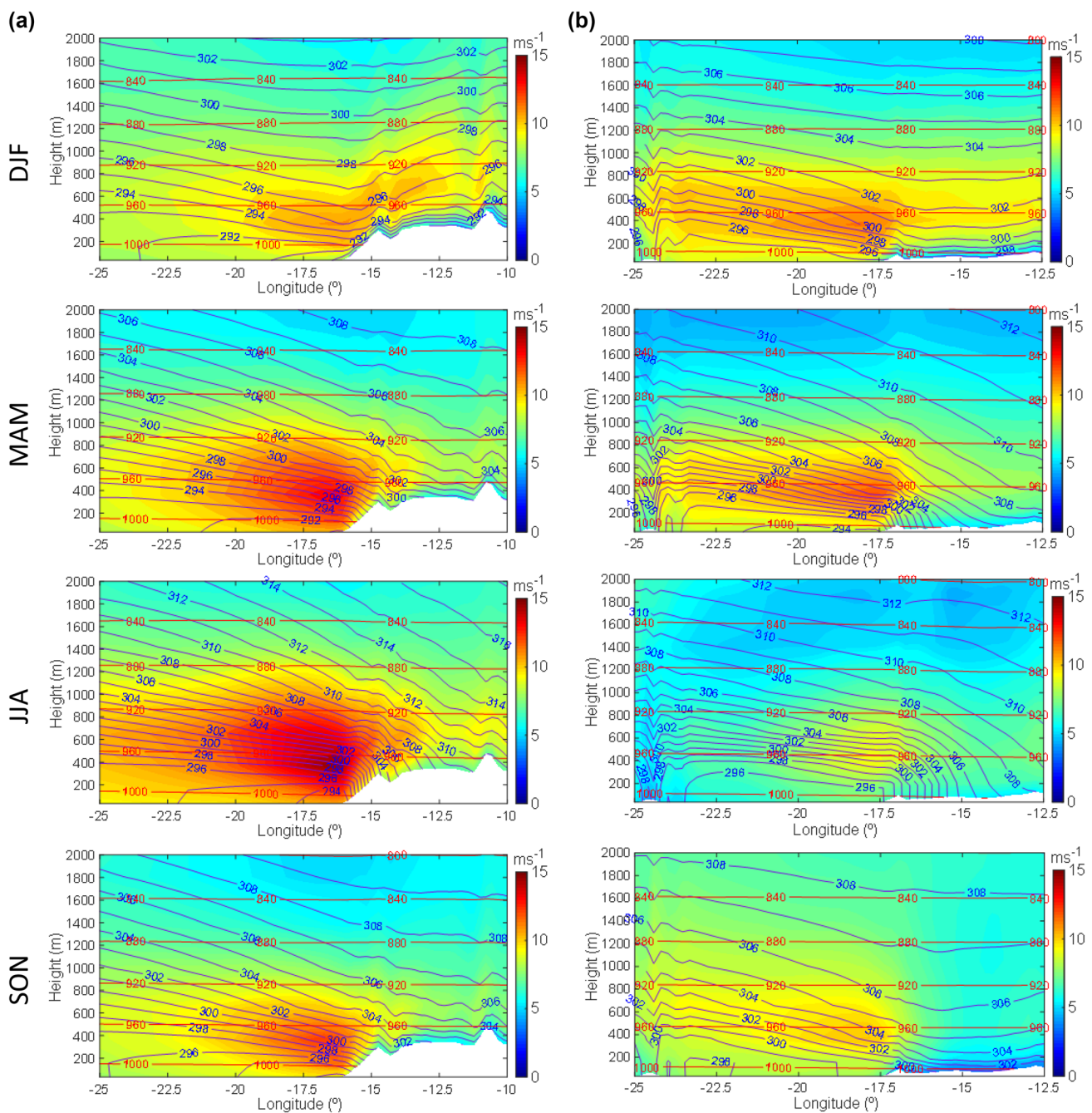


Fig. 9 Mean cross-sections when jet occurs for all seasons at **a** 23.76°N and **b** 14.74°N. Colors refer to mean jet wind speeds and contours to mean potential temperature (blue) and pressure (red)

(2005) indicate a semi-geostrophic balance for the meridional component and geostrophy in the case of the zonal jet wind component.

In summer, the pressure gradient (PG) and the Coriolis effect (CO), from the zonal momentum balance (Fig. 10), are the major terms in most of the region, revealing some degree of geostrophic balance in the CLLJ areas. The PG acceleration and the CO term show relative maxima, between the

two of the most striking coastal irregularities (Cape Rhir and Cape Blanc), and in the regions overlapping areas of maxima frequency of occurrence (Fig. 5) and of jet wind speed at 360 m (Fig. 12a). In general the horizontal advection and the mixing terms are negligible. Therefore, Eq. 11 can be simplified to: $\partial \bar{u} / \partial t = -f(\bar{V}_g - \bar{V})$, where $\bar{V}_g = 1/\rho f(\partial \bar{p} / \partial x)$.

In the regions of maximum frequency of occurrence (e.g. coastal offshore region of Western Sahara), the CO

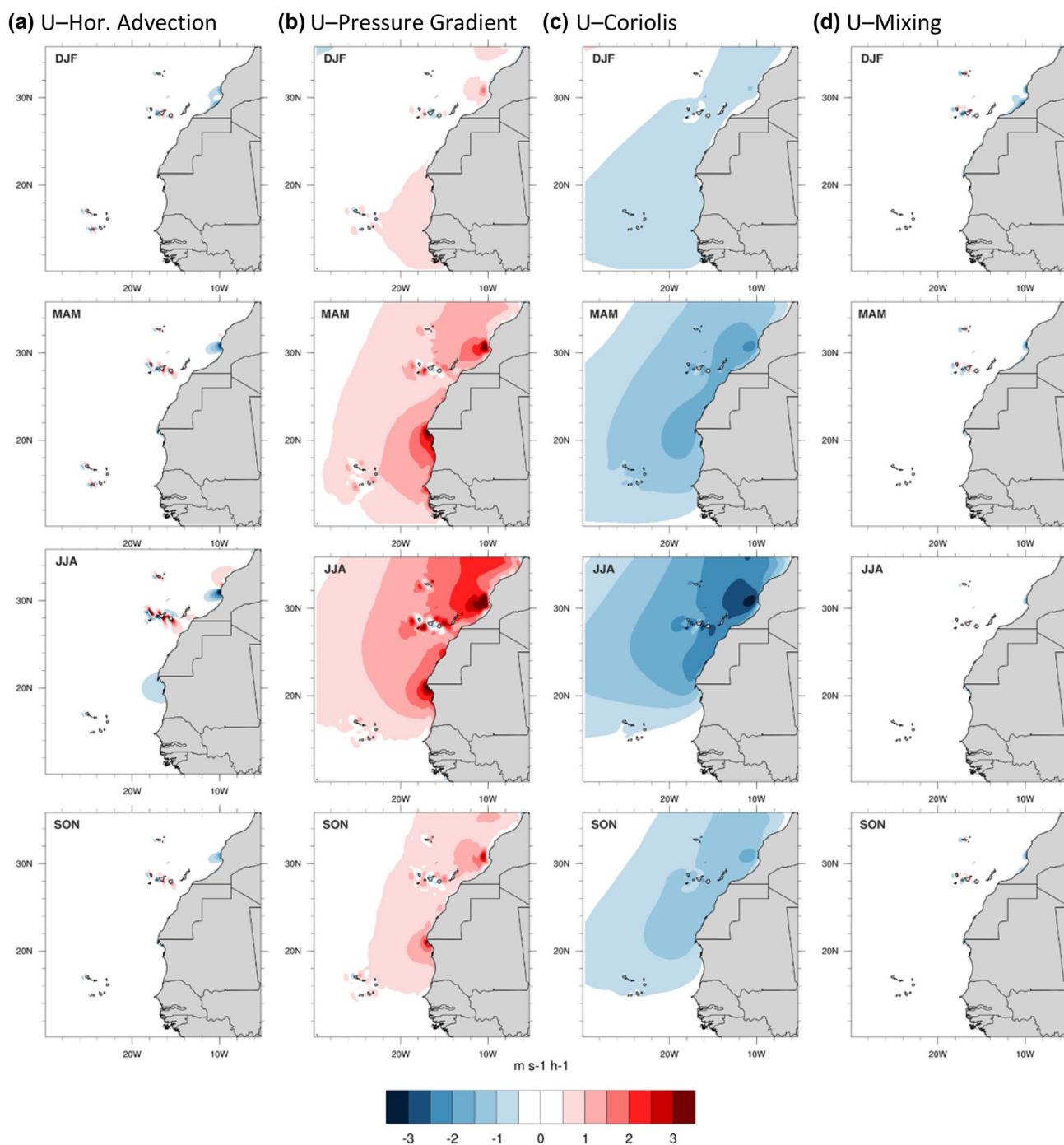


Fig. 10 Maps of seasonal terms of zonal momentum budget at 360 m a.s.l.: **a** horizontal advection, **b** pressure gradient, **c** Coriolis and **d** mixing terms ($\text{ms}^{-1}\text{h}^{-1}$)

term is somewhat larger than the PG term, indicating local negative ageostrophy (Fig. 12c, $V < V_g$), and subsequently the zonal acceleration that enhances the coastal jet. This is also visible downwind of the referred capes, yet here the horizontal advection contributes negatively to the balance, which results in to a maxima of the ageostrophic

meridional components (Fig. 12c) and zonal decelerating. This zonal component decrease is linked to an expansion fan process that enhances the meridional wind component, and the wind jet, due to coastal bending. In autumn, the horizontal momentum balance when the jet occurs follows a similar reasoning. However, in spring and

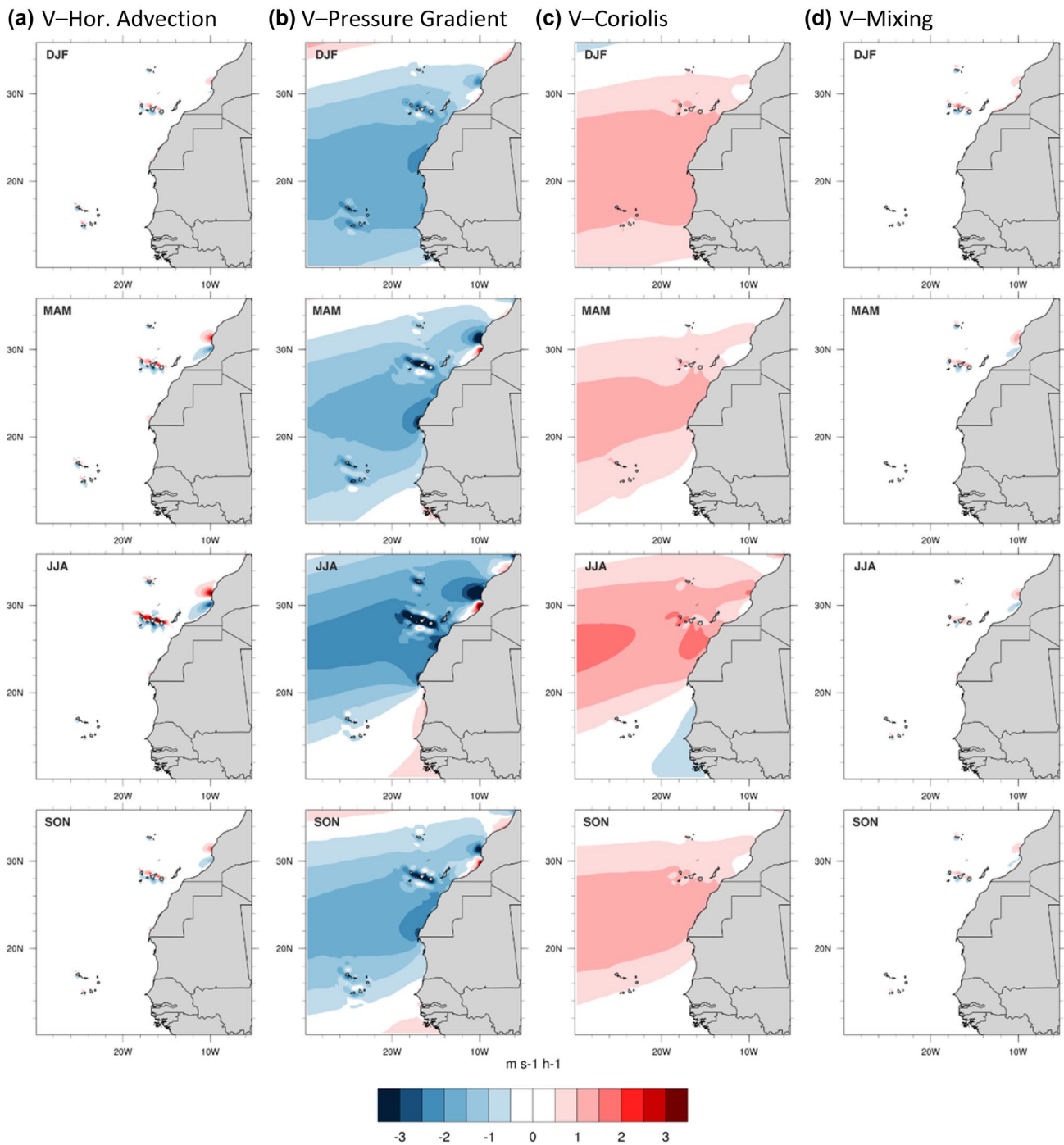


Fig. 11 Maps of seasonal terms of meridional momentum budget at 360 m a.s.l.: **a** horizontal advection, **b** pressure gradient, **c** Coriolis and **d** mixing terms ($\text{ms}^{-1}\text{h}^{-1}$)

winter, the jet appears displaced further south, where a quasi-geostrophic zonal balance takes place offshore and the ageostrophy is close to zero (Fig. 12c).

The meridional momentum balance is also dominated by the PG and the CO terms. These present a rather latitudinal pattern but with large pressure perturbations

associated to coastal main irregularities. The CO term, in a less extent, shows some regional maxima located as well in the main jet areas. The meridional horizontal advection and mixing terms are mostly negligible, except offshore of Cape Rhir. Similarly, Eq. 12 may be simplified to $\partial \bar{v} / \partial t = f(\bar{U}_g - \bar{U})$, where $\bar{U}_g = -1/\rho f(\partial \bar{p} / \partial y)$. In

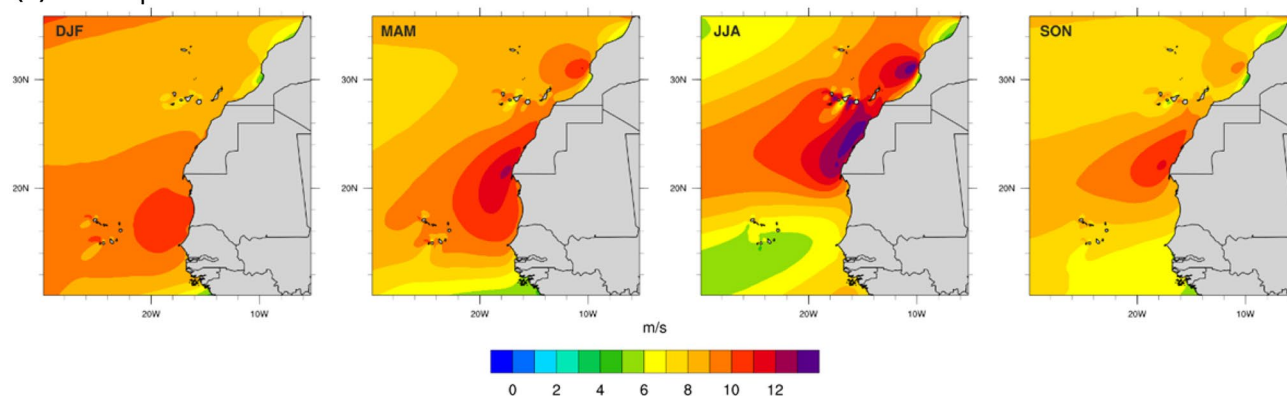
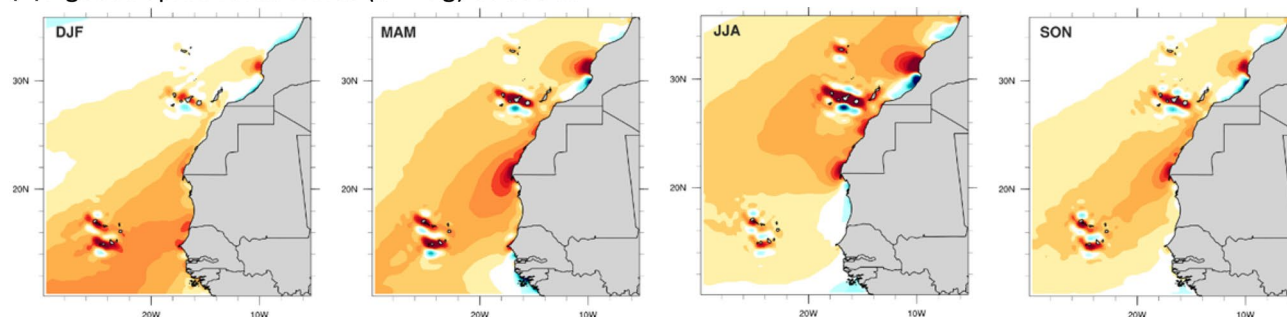
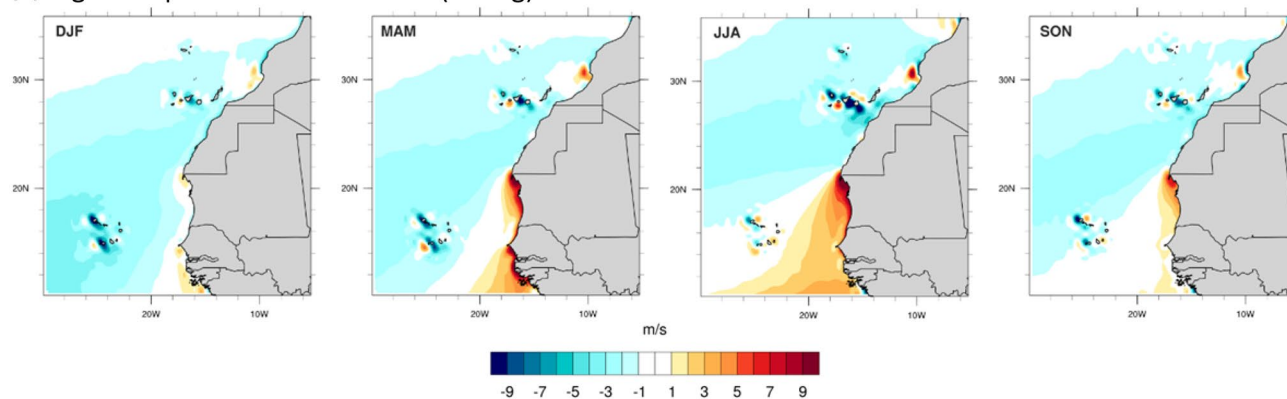
(a) Wind speed at 360 m**(b) Ageostrophic zonal winds ($U - U_g$) at 360 m****(c) Ageostrophic meridional winds ($V - V_g$) at 360 m**

Fig. 12 Maps of seasonal **a** wind speed, **b** zonal ageostrophic wind and **c** meridional ageostrophic wind at 360 m a.s.l (m/s), all when jet occurs

summer, most notably in the jet areas and where the horizontal advection is small, the meridional PG is in absolute value larger than the CO, which results in a positive ageostrophy (Fig. 12b) and in the meridional flow acceleration and the wind jet. In the remaining seasons the positive ageostrophy occurs further south.

3.4 Interannual variability

The recent evolution of the NACLLJ is illustrated through the seasonal time-series of the anomalies of the mean frequency of occurrence and of the mean jet wind speed

(Fig. 13). As previously shown, summer is the season when the jet is consistently more prevalent followed by spring, autumn and then winter. The inter-annual variability is however higher in spring than in summer. This is illustrated by the inter-annual standard deviations of the frequency of occurrence which are 2.47, 1.94, 1.57 and 1.44% for spring, summer, autumn and winter, respectively. Moreover, summer and spring show larger peak anomalies that do not occur in the remaining seasons, e.g. in spring anomalies can reach 6% with respect to the mean frequency of occurrence of 15.71%. The mean jet wind speed reveals a less degree of inter-annual variability. For

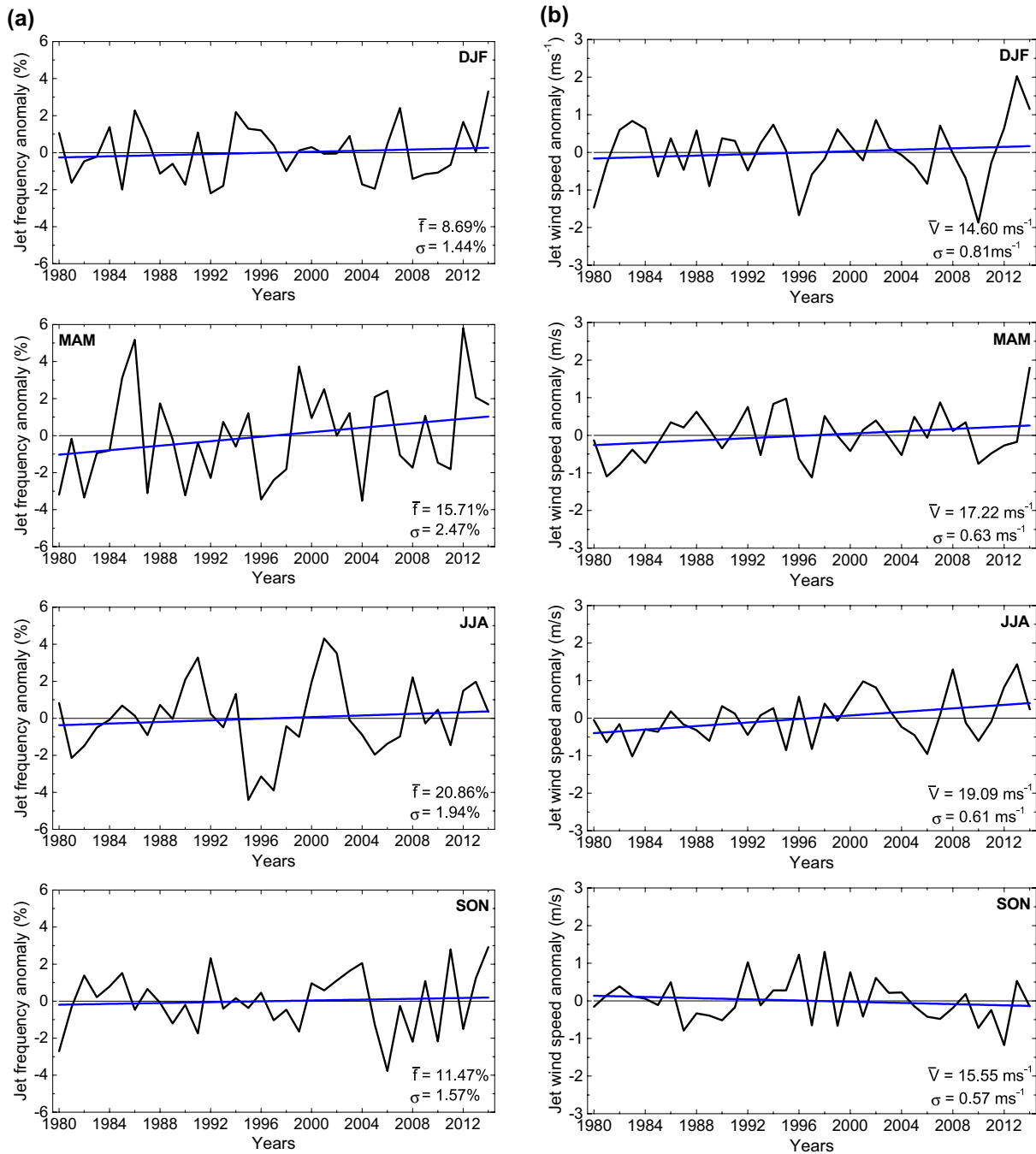


Fig. 13 Seasonal time series of the **a** jet frequency of occurrence and **b** jet wind speed

all seasons the standard deviations are smaller than 0.81%. In fact, the seasons with less frequency of jet occurrence are the ones presenting higher jet wind speed inter-annual variability.

Interestingly, the NACCLL occurrence seems to be increasing for all seasons, particularly in spring. Although

this trend is statistically significant, it should be seen prudently, since in some way depends on the last years of jet frequency records. The jet wind speed tendencies, for the full period, also points out to an increment of the seasonal jet winds speeds, with the exception of autumn.

4 Conclusions

In the Northeastern Atlantic basin, the Azores High pressure system sets synoptically alongshore flow offshore of western Iberia and western North Africa. This flow is regionally enhanced, especially in summer, by thermal lows over Iberia and over the North Africa. These give rise to the Iberian CLLJ and the NACLLJ, which are separated by the atmospheric flow off Gibraltar (Ranjha et al. 2013).

The main objective of the current study was to investigate the spatial and temporal features of the NACLLJ, which included the jet seasonal and diurnal cycles, the horizontal and vertical structures of the frequency of occurrence and jet wind speeds, the dynamical balance and the inter-annual variability. A high-resolution ROM hindcast simulation, at ~25 km resolution, for the 1980–2014 period, was used. Additionally, the underlying surface wind features were scrutinized, also recurring to the CORDEX-Africa runs. These runs allowed the building of a multi-model ensemble for the surface flow and exposed the models good performance to describe the flow spatial properties, from daily to yearly scales.

The NACLLJ showed a strong annual cycle, but unlike most CLLJs, e.g. the California and Iberia ones (Soares et al. 2014; Lima et al. 2018), it is expressively present all year round, with frequencies of occurrence above 20%. In spring and autumn the maxima frequencies are around 50%, and in summer reach values above 60%. These values are considerably higher than the ones suggested by Lima et al. (2018), a fact that is linked to the benefits of using high resolution downscaling for an improved representation of CLLJs (Ranjha et al. 2016). The maximum frequency of occurrence migrates from season to season, occurring in winter and spring upwind of Cap-Vert and in summer and autumn offshore Western Sahara. Similarly, the lower jet wind speeds occur in winter, when the median jet wind speed is below 15 m/s and the maximum jet wind speeds are below 28 m/s, and appear higher in summer, when median values rise to around 20 m/s and the jet wind speed maxima are above 30 m/s. The spatial extension of the NACLLJ is remarkable, spreading from the north offshore regions of Morocco (in all seasons with the exception of winter) to the southern offshore areas of Guineas. Furthermore, the offshore horizontal extension of the NACLLJ is for all year above 600 km, and is maximum in summer when it reaches areas more than 1200 km offshore the Western Saharan coast.

The jet vertical cross-sections showed the well-mixed MABL and the subsidence aloft that compresses the isentropes constraining the heights where the jet maxima occurs. The thermally direct circulation associated to the temperature contrast between land and ocean enhances the isothermal slope near the coast. The horizontal temperature

gradient and the associated thermal wind adjustment gives rise to the maxima of jet wind speed in the inversion layer. The heights of jet occurrence are quite similar from season to season, being more prevalent on heights around 360 m.

The momentum balance analysis disclosed that the flow is almost geostrophic, dominated by the pressure gradient and Coriolis force, with an overall negligible mixing and advection terms. The ageostrophy is higher over the jet areas and is responsible for the jet acceleration. Downwind of the most relevant capes, advection plays a role, decelerating the zonal wind component and enhancing the meridional wind component, and the wind jet, due to coastal bending in the expansion fan process.

The inter-annual variability of the NACLLJ is larger in spring than in the other seasons. In the last 35 years, with the exception of autumn, both the persistency and intensity of the jet have positive inter-annual variability trends. Particularly relevant are the increasing tendencies in spring and summer. Interestingly, Soares et al. (2017a) suggested large increases in the occurrence of the Iberian CLLJ in response to climate change, using a high resolution WRF simulation. Semedo et al. (2016) had also studied the global future changes of CLLJs persistency, and had also pointed to a projected increase for the NACLLJ. These evidences suggest the need for a deep analysis of the evolution of the NACLLJ connected with global warming and its impact on the regional climate.

Acknowledgements We thank two anonymous reviewers for their very helpful comments. Pedro M. M. Soares, Rita M. Cardoso and A. Semedo wish to acknowledge the SOLAR (PTDC/GEOMET/7078/2014) project. Daniela Lima also thanks the Earth-Systems Doctoral Programme at the Faculty of Sciences of the University of Lisbon (Grant PD/BD/106008/2014), without which this work would not have been possible. These authors also acknowledge the funding by the project FCT UID/GEO/50019/2013—Instituto Dom Luiz. D. Sein's work was supported by the PRIMAVERA project, which has received funding from the European Union's Horizon 2020 research and innovation programme under Grant agreement no. 641727 and the state assignment of FASO Russia (Theme 0149-2018-0014). Finally, all authors acknowledge the German Climate Computing Center (DKRZ) where the ROM simulations were performed, and are grateful to the World Climate Research Program Working Group on Regional Climate, and the Working Group on Coupled Modelling, former coordinating body of CORDEX and responsible panel for CMIP5. The authors also thank the climate modelling groups (listed in Table 1 of this paper) for producing and making available their CORDEX-Africa model output.

References

- Atlas R, Hoffman RN, Ardizzone J, Leidner SM, Jusem JC et al (2011) A cross-calibrated, multiplatform ocean surface wind velocity product for meteorological and oceanographic applications. *Bull Am Meteorol Soc* 92:157–174. <https://doi.org/10.1175/2010BAMS2946.1>

- Benazzouz A, Mordane S, Orbi A, Chagdali M, Hilmi K, Atillah A, Pelegri JL, Demarcq H (2014a) An improved coastal upwelling index from sea surface temperature using satellite-based approach—the case of the Canary Current upwelling system. *Cont Shelf Res* 81:38–54
- Benazzouz A, Pelegri JL, Demarcq H, Machin F, Mason E, Orbi A, Pena-Izquierdo J, Soumia M (2014b) On the temporal memory of coastal upwelling off NW Africa. *J Geophys Res Oceans* 119:6356–6380. <https://doi.org/10.1002/2013JC009559>
- Boberg F, Berg P, Thejll P, Gutowski WJ, Christensen JH (2009) Improved confidence in climate change projections of precipitation evaluated using daily statistics from the PRUDENCE ensemble. *Clim Dyn* 32(7–8):1097–1106. <https://doi.org/10.1007/s00382-008-0446-y>
- Bosilovich MG et al (2015) MERRA-2: initial evaluation of the climate. Technical Report Series on Global Modeling and Data Assimilation. 43. NASA/TM-2015-104606/Vol. 43
- Burk SD, Thompson WT (1996) The summertime low-level jet and marine boundary layer structure along the California coast. *Monthly Weather Rev* 124(4):668–686
- Cardoso RM, Soares PMM, Lima DCA, Semedo A (2016) The impact of climate change on the Iberian low-level wind jet: EURO-CORDEX regional climate simulation. *Tellus A* 68:29005. <https://doi.org/10.3402/tellusa.v68.29005>
- Cardoso RM, Soares PMM, Lima DCA, Miranda PMA (2018) Mean and extreme temperatures in a warming climate: EURO-CORDEX and WRF regional climate high-resolution projections for Portugal. *Clim Dyn*. <https://doi.org/10.1007/s00382-018-4124-4>
- Chao S (1985) Coastal jets in the lower atmosphere. *J Phys Oceanogr* 15:361–371
- Christensen OB, Drews M, Christensen JH, Dethloff K, Ketelsen K, Hebestadt I, Rinke A (2007) The HIRHAM regional climate model version 5 (beta). Technical Report 06-17, pp 1–22
- Dee DP et al (2011) The ERA-Interim reanalysis: configuration and performance of the data assimilation system. *Q J R Meteorol Soc* 137:553–597
- Ferro CAT, Hannachi A, Stephenson DB (2005) Simple nonparametric techniques for exploring changing probability distributions of weather. *J Clim* 18(21):4344–4354
- Findlater J (1969) A major low-level air current near the Indian Ocean during the northern summer. *Q J R Meteorol Soc* 95(404):362–380
- Giorgi F, Jones C, Asrar G (2009) Addressing climate information needs at the regional level: the CORDEX framework. *WMO Bull* 58:175–183
- Gómez-Gesteira M, De Castro M, Álvarez I, Lorenzo MN, Gesteira JLG, Crespo AJC (2008) Spatio-temporal upwelling trends along the Canary upwelling system (1967–2006). *Ann N Y Acad Sci*. <https://doi.org/10.1196/annals.1446.004>
- Hewitson B, Lennard C, Nikulin G, Jones C (2012) CORDEX-Africa: a unique opportunity for science and capacity building. CLIVAR Exchanges 60, International CLIVAR Project Office, Southampton, pp 6–7
- Jacob D et al (2001) A comprehensive model inter-comparison study investigating the water budget during the BALTEX-PIDCAP period. *Meteorol Atmos Phys* 77:19–43. <https://doi.org/10.1007/s007030170015>
- Kobayashi S et al (2015) The JRA-55 reanalysis: general specifications and basic characteristics. *J Meteorol Soc Jpn* 93:5–48
- Li M, Liu J, Wang Z, Wang H, Zhang Z, Zhang L, Yang Q (2013) Assessment of sea surface wind from NWP reanalyses and satellites in the Southern Ocean. *J Atmos Oceanic Technol* 30:1842–1853. <https://doi.org/10.1175/JTECH-D-12-00240.1>
- Lima DCS, Soares PMM, Semedo A, Cardoso RM (2018) A global view of coastal low-level wind jets using an ensemble of reanalysis. *J Clim* 31(4):1525–1546. <https://doi.org/10.1175/JCLI-D-17-0395.1>
- Martynov A, Laprise R, Sushama L, Winger K, Separovic L, Dugas B (2013) Reanalysis-driven climate simulation over CORDEX North America domain using the Canadian Regional Climate Model, version 5: model performance evaluation. *Clim Dyn* 41:2973–3005. <https://doi.org/10.1007/s00382-013-1778-9>
- Muñoz RC, Garreaud R (2005) Dynamics of the low-level jet off the west coast of subtropical South America. *Monthly Weather Rev* 133(12):3661–3677. <https://doi.org/10.1175/MWR3074.1>
- Nikulin G, Jones C, Samuelsson P, Giorgi F, Sylla MB, Asrar G, Büchner M, Cerezo-Mota R, Christensen OB, Déqué M, Fernandez J, Hañsler A, van Meijgaard E, Sushama L (2012) Precipitation climatology in an ensemble of CORDEX-Africa regional climate simulations. *J Clim*. <https://doi.org/10.1174/JCLI-D-11-00375.1>
- Nogueira M, Soares PMM, Tomé R, Cardoso RM (2018) High-resolution multi-model projections of onshore wind resources over Portugal under a changing climate. *Theor Appl Climatol*. <https://doi.org/10.1007/s00704-018-2495-4>
- Parish TR (2000) Forcing of the summertime low-level jet along the California Coast. *J Appl Meteorol* 39(12):2421–2433. [https://doi.org/10.1175/1520-0450\(2000\)039<2421:FOTSL>2.0.CO;2](https://doi.org/10.1175/1520-0450(2000)039<2421:FOTSL>2.0.CO;2)
- Perkins SE, Pitman AJ, Holbrook NJ, McAnaney J (2007) Evaluation of the AR4 climate models' simulated daily maximum temperature, minimum temperature, and precipitation over Australia using probability density functions. *J Clim* 20:4356–4376
- Ranjha R, Svensson G, Tjernström M, Semedo A (2013) Global distribution and seasonal variability of coastal low-level jets derived from ERA-Interim reanalysis. *Tellus A* 65:20412. <https://doi.org/10.3402/tellusa.v65i0.20412>
- Ranjha R, Tjernström M, Semedo A, Svensson G (2015) Structure and variability of the Oman coastal low-level jet. *Tellus A* 67:25285. <https://doi.org/10.3402/tellusa.v67.25285>
- Ranjha R, Tjernström M, Svensson G, Semedo A (2016) Modeling coastal low-level wind-jets: does horizontal resolution matter? *Meteorol Atmos Phys* 128:263–278. <https://doi.org/10.1007/s00703-015-0413-1>
- Rijo N, Lima DCA, Semedo A, Miranda PMA, Cardoso RM, Soares PMM (2017) Spatial and temporal variability of the Iberian Peninsula coastal low-level jet. *Int J Climatol* 38(4):1605–1622. <https://doi.org/10.1002/joc.5303>
- Rockel B, Will A, Hense A (2008) The regional climate model COSMO-CLM (CCLM). *Meteorologische Zeitschrift* 17:347–348
- Saha S et al (2010) The NCEP climate forecast system reanalysis. *Am Meteorol Soc* 91:1015–1057
- Samuelsson P et al (2011) The Rossby Centre Regional Climate model RCA3: model description and performance. *Tellus Ser A Dyn Meteorol Oceanogr* 63:4–23. <https://doi.org/10.1111/j.1600-0870.2010.00478.x>
- Sein DV, Mikolajewicz U, Groger M, Fast I, Cabos W, Pinto JG, Hagemann S, Semmler T, Izquierdo A, Jacob D (2015) Regionally coupled atmosphere-ocean-sea ice-marine biogeochemistry model ROM: 1. Description and validation. *J Adv Model Earth Syst* 7:268–304. <https://doi.org/10.1002/2014MS000357>
- Semedo A, Soares PMM, Lima DCA, Cardoso RM, Bernardino M, Miranda PMA (2016) The impact of climate change on the global coastal low-level wind jets: EC-EARTH simulations. *Glob Planet Change* 137:88–106
- Soares PMM, Cardoso RM, Miranda PMA, Medeiros J, De Belo-Pereira M and co-authors (2012) WRF high resolution dynamical downscaling of ERA-Interim for Portugal. *Clim Dyn* 39:24972522. <https://doi.org/10.1007/s00382-012-1315-2>
- Soares PMM, Cardoso RM, Semedo A, Chinista MJ, Ranjha R (2014) Climatology of Iberia coastal low-level wind jet: WRF high resolution results. *Tellus A* 66:22377. <https://doi.org/10.3402/tellusa.v66.22377>

- Soares PMM, Cardoso RM, Ferreira JJ, Miranda PMA (2015) Climate change and the Portuguese precipitation: ENSEMBLES regional climate model results. *Clim Dyn* 45(7):1771–1787. <https://doi.org/10.1007/s00382-014-2432-x>
- Soares PMM, Lima DCA, Cardoso RM, Semedo A (2017a) High resolution projections for the western Iberian coastal low level jet in a changing climate. *Clim Dyn*. <https://doi.org/10.1007/s00382-016-3397-8>
- Soares PMM, Cardoso RM, Lima DCA, Miranda PMA (2017b) Future precipitation in Portugal: high-resolution projections using WRF model and EURO-CORDEX multi-model ensembles. *Clim Dyn* 49:2503–2530. <https://doi.org/10.1007/s00382-016-3455-2>
- Soares PMM, Lima DCA, Cardoso RM, Nascimento M, Semedo A (2017c) Western Iberian offshore wind resources: more or less in a global warming climate? *Appl Energy* 203:72–90. <https://doi.org/10.1016/j.apenergy.2017.06.004>
- Tang WQ, Liu WT, Stiles BW (2004) Evaluations of high resolution ocean surface vector winds measured by QuikSCAT scatterometer in coastal regions. *IEEE Trans Geosci Remote Sens* 42:17621769
- Tjernström M, Grisogono B (2000) Simulations of supercritical flow around points and capes in the coastal atmosphere. *J Atmos Sci* 52:863–878
- van Meijgaard E, Van Uft LH, Van De Berg WJ, Bosveld FC, Van Den Hurk BJM, Lenderink G, Siebesma AP (2008) The KNMI regional atmospheric climate model RACMO version 2.1. Koninklijk Nederlands Meteorologisch Instituut, 43
- Willmott CJ, Robeson SM, Matsuura K (2012) A refined index of model performance. *Int J Climatol* 32:2088–2094
- Winant CD, Dorman CE, Friehe CA, Beardsley RC (1988) The marine layer off northern California: an example of supercritical channel flow. *J Atmos Sci* 45:3588–3605